

## THE NORMALIZED EMISSION SPECTRUM OF THE EFFECTIVE ATOM-PHOTON-MAGNON SYSTEM

by

**Hanaa ABU-ZINADAH<sup>a,\*</sup> and Eied Mahmoud KHALIL<sup>b,c</sup>**

<sup>a</sup>Department of Mathematics and Statistics, College of Science,  
University of Jeddah, Jeddah, Saudi Arabia

<sup>b</sup>Department of Mathematics, College of Science, Taif University, Taif, Saudi Arabia

<sup>c</sup>Mathematics Department, Faculty of Science, Al-Azhar University, Cairo, Egypt

Original scientific paper

<https://doi.org/10.2298/TSCI2406831A>

*This paper explores the behaviour of the normalized emission spectrum within the confines of the atom-photon-magnon regime at its dispersive limit, with a focus on its dependency on various parameters and initial conditions. The investigation reveals several significant findings. Firstly, regarding the mixing angle and detuning, minimal variation in the spectrum is observed with small detuning values, although the influence of the mixing angle becomes more pronounced for the initial squeezed coherent and initial binomial states, particularly notable in the case of the squeezed coherent state. Secondly, concerning the initial state strength, an increase in strength results in a gradual decrease in the spectrum across all states except the binomial state, which finally experiences an increase. However, the squeezed coherent state displays a gradual decay without reaching zero, whereas the thermal state decays completely. Lastly, concerning magnon-cavity coupling, stronger coupling between magnon and cavity causes a shift in the spectrum towards higher positive detuning, with a more pronounced shift observed in the squeezed coherent state compared to other states.*

Key words: *dispersive limit, atom-photon-magnon, emission spectrum, binomial state, squeezed coherent state, thermal state*

### Introduction

The atomic emission spectrum serves as a fundamental tool in characterizing the light emitted through the interaction between atomic radiation and the field [1, 2]. Experimentally, the emission spectrum of the two-color excitation state is very different from the characteristic triple emission spectrum that was seen in the case of strong single-mode field excitation [3]. Further investigations have employed continuous fraction methods to address system equations for the dipole-dipole correlation functions, where these methods were instrumental in calculating the emission spectrum originating from a dipole [4]. The non-resonance case leads to an increase in the placed of atomic linewidth compared to the state of the resonance case [5]. A crucial threshold is reached when the interaction's magnitude surpasses that of the atomic and cavity fields, marking the onset of reversible spontaneous emission – a phenomenon known as vacuum Rabi oscillation [6]. Significant advancements in achieving strong coupling have been

\* Corresponding author, e-mail: [hhabuznadah@uj.edu.sa](mailto:hhabuznadah@uj.edu.sa)

demonstrated across diverse systems, notably in scenarios involving Rydberg atoms within microwave cavities [6], alkali metal atoms in photonic cavities [7], and semiconducting devices [8]. These achievements have paved the way for pivotal experiments within the realm of quantum information. Moreover, the emission spectrum of the vacuum field Rabi model of a single two-level atom in an optical quantized field has been observed [9-11]. Furthermore, comprehensive analyses have been conducted on the spectrum exhibited by a single two-level atom interacting with non-degenerate two-photon and multi-mode cavity fields [12, 13]. For a three-level atom and quantized field the cavity-field spectrum and the emission have been studied [14]. In the presence of non-linearities and stark shift absorption spectra and the fluorescence of atom-field interaction are discussed [15, 16]. Moreover, an in-depth scrutiny into the transient Haar wavelet spectrum of the pulsed harmonic oscillator and pulsed two-level atom has been analyzed [17, 18].

Over the past decade, hybrid quantum systems have garnered substantial interest among physicists and engineers, presenting a fertile ground for the implementation of contemporary quantum information tasks [19], quantum computing protocols [20], and state engineering [21]. On one hand, these hybrid quantum systems encompass diverse configurations involving interactions between light and matter. For examples, magnon-superconducting qubit [22], qubit-photon-magnon-quantum systems [23, 24], and qubit-photon-graphene [25-27]. These systems demonstrate intricate combinations where components interact, forming alliances such as magnon-photon-phonon [28], microwave photon-magnon-systems [29], or optomechanical-magnetic system [30-32]. On the other hand, recent studies have successfully verified the properties of these systems through various experimental set-ups. For instance, the achievement of strong coupling between magnon-s and photons at room temperature, highlighting the potential for coherent interactions within the system has demonstrated [33]. Entanglement based on superconducting circuits with the single-photon detector counterpart for magnon-ics is detected [34]. an optomechanical system utilizing two linked cavities and a high frequency microwave resonator to establish a controllable and powerful long-distance interaction between a single spin qubit and a magnon-within a YIG nanosphere is proposed [35].

This paper's central focus revolves around a comprehensive examination of the normalized emission spectrum inherent in a hybrid quantum system emerging from the interplay among atoms, photons, and magnons. The inquiry extensively explores varied initial states, particularly emphasizing the atom's initiation in an excited state while configuring the photon and magnon-states into diverse arrangements, such as binomial, squeezed coherence, or thermal states. The primary objective is to elucidate the diverse emission spectrum manifestations arising from distinctive initial conditions within this intricate quantum setting. The deliberate choice of different initial states serves as a potent instrument to unveil the multi-dimensional facets of our hybrid quantum system. Through meticulous selection and analysis of the system's response across varied initial conditions, we aim to further our understanding of the system's behaviour and could potentially unlock new vistas in quantum technologies.

### Physical model

In this section, we consider a hybrid physical quantum system comprising a superconducting qubit (single atom), a ferromagnetic crystal in the Kittel mode (a collective spin excitation), and a resonator (photon). The magnon-mode interacts with the resonator via the magnetic dipole interaction, while the single qubit is coupled to the resonator through a general Rabi model. The physical Hamiltonian of this system can be written [36]:

$$\hat{H} = \omega_c \hat{a}^\dagger \hat{a} + \omega_m \hat{m}^\dagger \hat{m} + \frac{\omega_q}{2} \hat{S}_z + \lambda_1 (\hat{a}^\dagger + \hat{a})(\hat{m}^\dagger + \hat{m}) + \lambda_2 (\hat{a}^\dagger + \hat{a})(\hat{S}_x \cos \theta + \hat{S}_z \sin \theta) \quad (1)$$

where  $\omega_c$ ,  $\omega_m$ , and  $\omega_q$  are the eigen-frequencies of the resonator, magnon-and qubit, respectively,  $\hat{a}^\dagger(\hat{a})$  and  $\hat{m}^\dagger(\hat{m})$  – the creation (annihilation) operators of the resonator and magnon-modes, respectively,  $\hat{S}_x$  and  $\hat{S}_z$  – the standard Pauli operators, which they are labeled by the excited ( $|e\rangle$ ), and the ground state ( $|g\rangle$ ):

$$\hat{S}_x = |e\rangle\langle g| + |g\rangle\langle e| \text{ and } \hat{S}_z = |e\rangle\langle e| - |g\rangle\langle g|$$

the  $\lambda_i$ ,  $i = 1, 2$  are coupling strengths of photon-magnon, qubit-photon, respectively. Despite previous demonstrations of strong magnon-cavity coupling in larger YIG spheres and the qubit-cavity coupling is a weak-coupling regime, this work assumes a weak-coupling regime for both the spin-cavity and magnon-cavity interactions due to the smaller YIG nanosphere being employed [37, 35]. Moreover, the angle,  $\theta$ , represents the transversal couplings and mixture of the longitudinal between the qubit and the cavity. The  $\theta$  exhibits broken parity-symmetry potential (evidenced by the  $\cos \theta$  factors); when  $\theta = 0$ , it reduces to the Jaynes-Cummings model with a magnon-mode, while circuit-QED experiments demonstrate the potential for ultrastrong coupling through an arbitrary mixture of longitudinal and transversal couplings [38, 39, 24].

The Hamiltonian (1) can be re-written under the rotating wave approximation:

$$\hat{\mathcal{H}} = \omega_c \hat{a}^\dagger \hat{a} + \omega_m \hat{m}^\dagger \hat{m} + \frac{\omega_q}{2} \hat{S}_z + \lambda_1 (\hat{a}^\dagger \hat{m} + \hat{m}^\dagger \hat{a}) + \lambda_2 \cos(\theta)(\hat{a} \hat{S}_+ + \hat{a}^\dagger \hat{S}_-) + \lambda_2 \sin(\theta)(\hat{a} + \hat{a}^\dagger) \hat{S}_z \quad (2)$$

In the interaction picture, the physical Hamiltonian model (2) can be obtained:

$$\begin{aligned} \hat{\mathcal{H}}_{IP} = & \lambda_1 \left[ \hat{m}^\dagger \hat{a} e^{i(\omega_m - \omega_c)} + \hat{a}^\dagger \hat{m} e^{-i(\omega_m - \omega_c)} \right] + \lambda_2 \cos(\theta) \left[ \hat{a} \hat{S}_+ e^{i(\omega_q - \omega_c)} + \hat{a}^\dagger \hat{S}_- e^{-i(\omega_q - \omega_c)} \right] + \\ & + \lambda_2 \sin(\theta) \left( \hat{a} e^{-i\omega_c} + \hat{a}^\dagger e^{i\omega_c} \right) \hat{S}_z \end{aligned} \quad (3)$$

Within the realm of dispersive interactions inherent in the hybrid model, it is assumed that the coupling strengths, represented by  $\lambda_1$  and  $\lambda_2$ , significantly pale in comparison the transition frequencies denoted as  $|\omega_m - \omega_c|$  and  $\omega_c$ , where  $\lambda_1, \lambda_2 \ll \omega_c$  and  $|\omega_m - \omega_c|$ . This assumption is made under the condition that  $\omega_m = \omega_q = \omega$  [40]. Consequently, the effective Hamiltonian governing the system takes the following form [41] (The detailed calculations is given in the Appendix A):

$$\hat{\mathcal{H}}_{eff} = \begin{bmatrix} (\alpha_1 + \alpha_2) \hat{a}^\dagger \hat{a} + \alpha_2 \hat{m}^\dagger \hat{m} + \alpha_1 + \alpha_3 & \alpha_4 \hat{m} \\ \alpha_4 \hat{m}^\dagger & (\alpha_2 + \alpha_1) \hat{a}^\dagger \hat{a} - \alpha_2 \hat{m}^\dagger \hat{m} + \alpha_3 \end{bmatrix} \quad (4)$$

where

$$\alpha_1 = -\frac{\lambda_2^2}{\omega_{11}} \cos^2(\theta), \quad \alpha_2 = \frac{\lambda_2^2}{\omega_{11}}, \quad \alpha_3 = \frac{\lambda_2^2}{\omega_{11}} \sin^2(\theta), \quad \text{and } \alpha_4 = \frac{-\lambda_1 \lambda_2}{\omega_{11}} \cos^2(\theta), \quad \text{with } \omega_{11} = \omega - \omega_c$$

It is easy to find the eigenenergies of the effective Hamiltonian (4), which get:

$$E_{\pm}^{n,m} = \frac{\alpha_1}{2} + \alpha_2 \left[ n - \left( m + \frac{1}{2} \right) \right] + \alpha_3 \pm \mu_{n,m} \quad (5)$$

with

$$\mu_{n,m}^2 = \frac{[\alpha_1 (2n+1) + \alpha_2]^2}{4} + (1+m) \alpha_4^2$$

with the corresponding eigenvectors:

$$\begin{aligned} |\Psi_+^n\rangle &= \sin \phi_{n,m} |n, m, e\rangle + \cos \phi_{n,m} |n, m+1, g\rangle \\ |\Psi_-^n\rangle &= \cos \phi_{n,m} |n, m, e\rangle - \sin \phi_{n,m} |n, m+1, g\rangle \end{aligned} \quad (6)$$

where

$$\tan \phi_{n,m} = \frac{2\alpha_4 \sqrt{m+1}}{\alpha_1(1+2n) + \alpha_2 - \mu_{n,m}}$$

On the other hand, the time-dependent emission spectrum of the a quantum system is expressed [42]:

$$S(\chi, T, \gamma) = 2\gamma \int_0^T dt' \int_0^T dt e^{-(T-t')(\gamma-i\chi) - (T-t)(\gamma+i\chi)} \langle \psi(0) | S^+(t') S(t) | \psi(0) \rangle \quad (7)$$

where  $\gamma$  is the Fabry detector width,  $T$  – the time measurement,  $\chi$  – the detector's detuning parameter, and  $|\psi(0)\rangle$  – the initial state of the system.

Now, we consider the atomic system is initially prepared in the excited state  $|e\rangle$ , while the initial photon and magnon-modes are initially considered:

$$|\eta\rangle = \sum_{n,m} b_n b_m |n, m\rangle$$

where  $b_i$ ,  $i = n, m$  is the number-state expansion coefficient. Thus, the initial state of the system is given:

$$|\psi(0)\rangle = \sum_{n,m} b_n b_m |n, m, e\rangle \quad (8)$$

The explicit analytical solution of time-dependent emission spectrum reads:

$$\begin{aligned} S(\epsilon, T, \gamma) &= 2\gamma \sum_{n,m} |b_n|^2 |b_m|^2 \left\{ \left| \cos \phi_{n,m} \cos^2 \phi_{n,m+1} C_1^+ + \cos \phi_{n,m} \sin^2 \phi_{n,m+1} C_1^- \right|^2 + \right. \\ &\quad \left. + \left| \sin \phi_{n,m} \cos^2 \phi_{n,m+1} C_2^+ + \sin \phi_{n,m} \sin^2 \phi_{n,m+1} C_2^- \right|^2 \right\} \end{aligned} \quad (9)$$

where

$$C_1^\pm = \frac{e^{-iT \left[ \epsilon \pm \frac{1}{2} (\mu_{n,m+1} \pm \mu_{n,m}) \right]} - e^{-\gamma T}}{\gamma - i \left[ \epsilon \pm \frac{1}{2} (\mu_{n,m+1} \pm \mu_{n,m}) \right]}, \quad C_2^\pm = \frac{e^{-iT \left[ \epsilon \pm \frac{1}{2} (\mu_{n,m+1} \mp \mu_{n,m}) \right]} - e^{-\gamma T}}{\gamma - i \left[ \epsilon \pm \frac{1}{2} (\mu_{n,m+1} \mp \mu_{n,m}) \right]} \quad (10)$$

with  $\epsilon = \chi - \alpha_2$  is the detuning parameter of the emission spectrum.

Hereinafter, we will use different initial states for both photons and magnons, characterized by their number distribution. Specifically, the state  $|\eta\rangle$  can be prepared as a binomial state, a squeezed coherent state, or a thermal state.

## Discussion

In this section, we will concentrate our attention on the influence of the initial distributions and different couplings on the normalized atomic emission spectrum. The normalized spectrum is defined [18]:

$$\mathcal{N}_S(\epsilon, T, \gamma) = \frac{S(\epsilon, T, \gamma)}{S_{\max}} \quad (11)$$

where  $S(\epsilon, T, \gamma)$  is the given by eq. (9) while  $S_{\max}$  is the obtained numerically. In investigation we will use the experimentally feasible frequencies parameters  $\omega_c/2\pi = 75$  GHz,  $\omega/2\pi = 7.2$  GHz, and  $t$  in nanosecond [22, 34]. However,  $\lambda_2 = 0.8\lambda_1$  which in GHz, and  $\gamma = 1$  nm for all studied states.

### Effect of binomial state

In this subsection, we consider the initial states of the photon and magnon as a binomial state, where the amplitude of the number state is given:

$$|b_\nu|^2 = \frac{\nu!}{M!(\nu-M)!} \eta^\nu (1-|\eta|)^{M-\nu} \quad (12)$$

where  $M$  is the positive integer number, and  $|\eta| \leq 1$ . In this state, as  $|\eta|$  increases the photon number  $\bar{n}$  increases, where  $\bar{n} = M|\eta|$ .

In fig.1, the computational results illustrating the normalized emission spectrum concerning the initial binomial state against the special detuning  $\epsilon$  are displayed. The spectrum depicted in fig. 1(a) exhibits a clear dependence on both the special detuning  $\epsilon$  and the mixing angle,  $\theta$ , where maintaining fixed parameters with  $\lambda_1/2\pi = 0.16$  GHz,  $\lambda_2 = 0.8\lambda_1$ ,  $T = 0.1$ , and  $\eta = 0.5$ . Notably, there is evident symmetry around  $\theta = \pi/2$ , with a discernible two peaks occurring at  $\theta = \pi/2$ , signifying weak coupling according to the Jaynes-Cummings model ( $\theta = 0, \pi$ ). Conversely, no spectrum is observable for large negative  $\epsilon$  values, while for positive  $\epsilon$  values, the spectrum is confined to small ranges. Figure 1(b) illustrates the spectrum's behavior concerning  $\epsilon$  and the  $\eta$  parameter with  $\lambda_1/2\pi = 0.16$  GHz,  $\lambda_2 = 0.8\lambda_1$ ,  $T = 0.1$ , and  $\theta = \pi/4$ . It is apparent that smaller values of  $\eta$  correspond to the maximum spectrum, which subsequently diminishes as  $\eta$  increases before exhibiting a resurgence at its maximum value. Moreover, an increase in  $\eta$  also leads to the appearance of a spectrum at positive  $\eta$  values. Figure 1(c) displays the normalized spectrum, portraying its dependence on the coupling of the magnon-photon  $\lambda_1$  and the special detuning  $\epsilon$ , where  $\lambda_2 = 0.8\lambda_1$ ,  $T = 0.1$ ,  $\eta = 0.5$ , and  $\theta = \pi/4$ . Initially, the spectrum exhibits two peaks symmetrically situated around the axis  $\epsilon = 0$ . However, as  $\lambda_1$  escalates, these peaks gradually coalesce, resulting in a reduction of the spectrum's maximum values. Concurrently, there is a positive shift observed in the spectrum with the increasing values of  $\epsilon$ . This observed shift could be ascribed to the interrelation between the  $\epsilon$  and the coupling of the magnon-photon. Figure 1(d) presents the spectrum concerning  $\epsilon$  and time,  $T$ , measured in nanoseconds, with  $\lambda_1/2\pi = 0.16$  GHz  $\lambda_2 = 0.8\lambda_1$ ,  $T = 0.1$ , and  $\theta = \pi/4$ . Notably, a complete symmetry is discerned in the resulting spectrum around the axis  $\epsilon \simeq 5$  GHz. Initially, two peaks emerge, yet fail to attain the maximum value of the spectrum. However, over time, these peaks amalgamate into a singular peak, centrally aligned along the axis  $\epsilon \simeq 5$  GHz, ultimately reaching the spectrum's maximum value.

### Effect of squeezed coherent state

Let us consider the scenario where the initial states of the field and magnon-are prepared in a squeezed state. In this context, the distribution of photon and magnon-numbers can be expressed:

$$|b_\nu|^2 = \left| H_\nu \left( \frac{\zeta}{\sqrt{2} \cosh r \sin r} \right) \right|^2 \frac{\tanh^\nu r}{2^\nu \nu! \cosh r} e^{-|\zeta|^2 + \tanh r \operatorname{Re}[\zeta]} \quad (13)$$

where  $\nu$  is the number state  $n$  or  $m$ ,  $H_\nu(\bullet)$  – the Hermite polynomial,  $\zeta = \beta \cos r + \beta^* \sinh r$ ,  $\beta$  – the intensity of squeezed state, and  $r$  – the setting parameter of the state, where one can get the coherent state at  $r = 0$ , whereas, the squeezed vacuum state may be generated for  $\beta = 0$ .

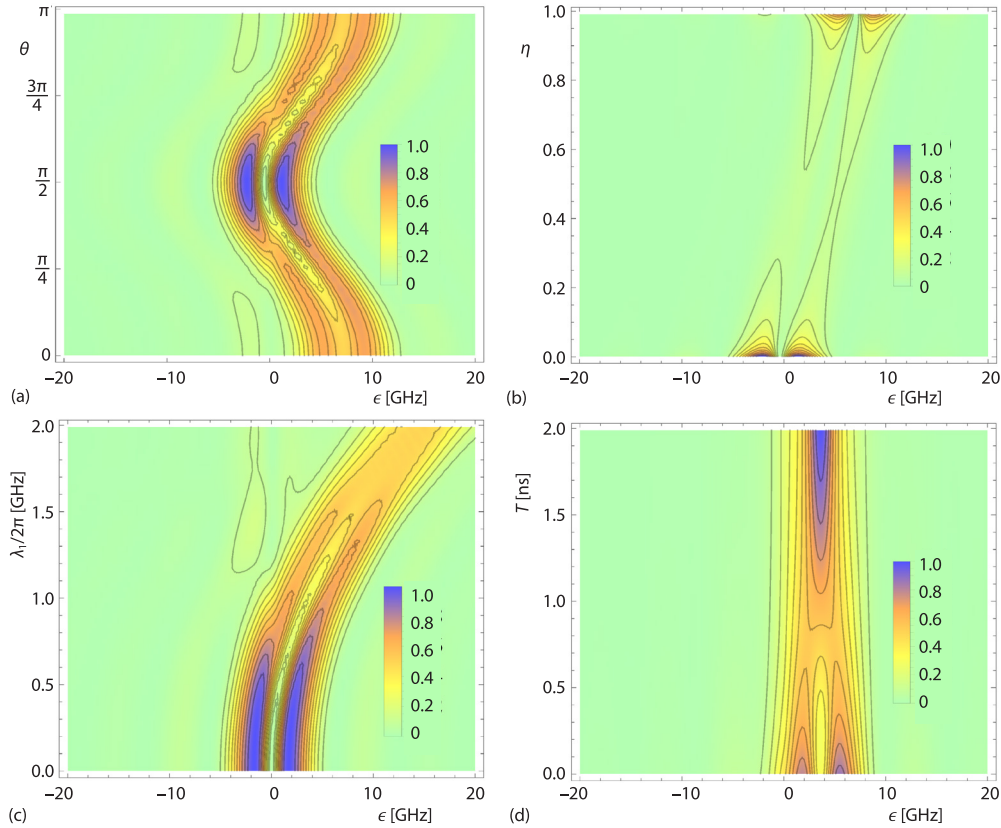


**Figure 1. The behavior of  $\mathcal{N}_S(\epsilon, T, \gamma)$  for the initial binomial state;**  
 (a)  $\lambda_1/2\pi = 0.16$  GHz,  $T = 0.1$ , and  $\eta = 0.5$ , (b)  $\lambda_1/2\pi = 0.16$  GHz,  $T = 0.1$ , and  $\theta = \pi/4$ ,  
 (c)  $T = 0.1$ ,  $\eta = 0.5$ , and  $\theta = \pi/4$ , (d)  $\lambda_1/2\pi = 0.16$  GHz,  $\eta = 0.5$ , and  $\theta = \pi/4$

The impact of the initial squeezed coherent state on the emission spectrum is elucidated in fig. (2), where diverse parameter configurations are examined. It becomes apparent that the emission spectrum in the initial squeezed coherent state bears striking resemblance to that in the binomial state, yet displaying a notably intricate structure within the two side peaks [43]. In fig. 2(a), the squeezed parameter,  $r$ , delineates, within the  $(\theta - \epsilon)$  plane, a notable resemblance of the two side peaks to the binomial state when theta equals  $\pi/2$ , exhibiting symmetric behavior around the axis  $\theta = 0$ . However, these two peaks merge and shift towards positive epsilon. It is also worth mentioning that a small mixing angle,  $\theta$ , yields a diverse and intricate spectrum. Additionally, figs. 2(b) and 2(c) show a discernible trend as the strength of the squeezed coherent parameter,  $\zeta$ , and the magnon-field coupling  $\lambda_1$  increase, wherein the two side peaks gradually diminish from the vacuum field Rabi peak, also referred to as the two master peaks. Interestingly, the shift induced by the increase in  $\lambda_1$  within the squeezed coherent state appears relatively larger than the shift observed in the binomial state. In fig. 2 (d), a similar pattern is observed for the spectrum in the  $\epsilon - T$  plane between the binomial state and the squeezed coherent state, however, the  $r$ , alters the position of the master peaks. This underscores the sensitivity of the emission spectrum to subtle variations in the initial state parameters.

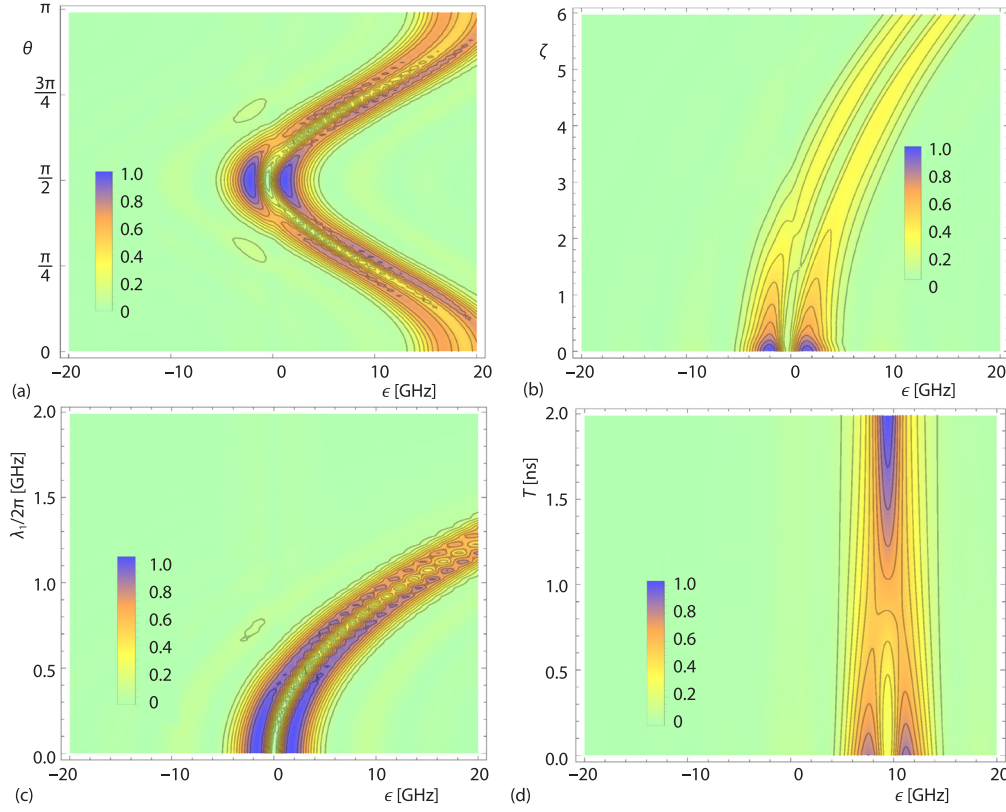


**Figure 2.** The behavior of  $\mathcal{N}_s(\epsilon, T, \gamma)$  for the initial squeezed coherent state with  $r = 1.5$ ; (a)  $\lambda_1/2\pi = 0.16$  GHz,  $T = 0.1$ , and  $\zeta = 5$ , (b)  $\lambda_1/2\pi = 0.16$  GHz,  $T = 0.1$ , and  $\theta = \pi/4$ , (c)  $T = 0.1$ ,  $\zeta = 5$ , and  $\theta = \pi/4$ , and (d)  $\lambda_1/2\pi = 0.16$  GHz,  $\zeta = 5$ , and  $\theta = \pi/4$

### Effect of thermal state

In this subsection, we will display the effect of the initial thermal state on the emission spectrum, where the geometrical amplitude of this state is given:

$$|b_\nu|^2 = \frac{\bar{n}^\nu}{(1 + \bar{n})^{\nu+1}} \quad (14)$$

where  $\bar{n}$  is the photon number distribution.

The investigation presented in fig. 3 reveals distinct characteristics of the normalized emission spectrum when initializing the magnon-and photon fields within an initial thermal state. The features displayed by each peak are contingent upon the intricate interplay among parameters such as  $\theta$ ,  $\bar{n}$ ,  $\lambda_1$ , and  $T$ . This configuration yields a complex spectrum, characterized by two adjacent peaks in different planes at lower values of system parameters. Figure 3(a) illustrates that the spectrum in the  $(\epsilon - \theta)$  plane undergoes more pronounced changes in the positive,  $\epsilon$ , region with varying mixing angle,  $\theta$ , compared to the negative,  $\epsilon$ , region. Notably, the shift observed in the previous two cases is absent in the thermal state, with the spectrum reaching its maximum value at  $3\pi/4 > \theta > \pi/4$ . Figure 3(b) depicts the spectrum in the  $(\epsilon - \bar{n})$  plane, revealing a gradual decay and eventual disappearance of the spectrum with in-

creasing  $\bar{n}$ . Thus, selecting smaller values of  $\bar{n}$  becomes imperative to mitigate spectrum decay. Furthermore, fig. 3(c) portrays the spectrum in the  $(\epsilon - \lambda_1/2\pi)$  plane, demonstrating that while the spectrum initially shows minimal dependence on  $\lambda_1$  when  $\lambda_1/2\pi < 1$ , it disperses and broadens as  $\lambda_1$  increases, accompanied by a reduction in the maximum value. This observation suggests a potential violation of the dispersive limit condition. In fig. 3(d), the spectrum in the  $(\epsilon - T)$  plane displays no shift in spectral regions, unlike figs. 1(d) and 2(d). This indicates that the spectrum remains unaffected by the  $\alpha_2$  coupling, responsible for shifts in this plane.

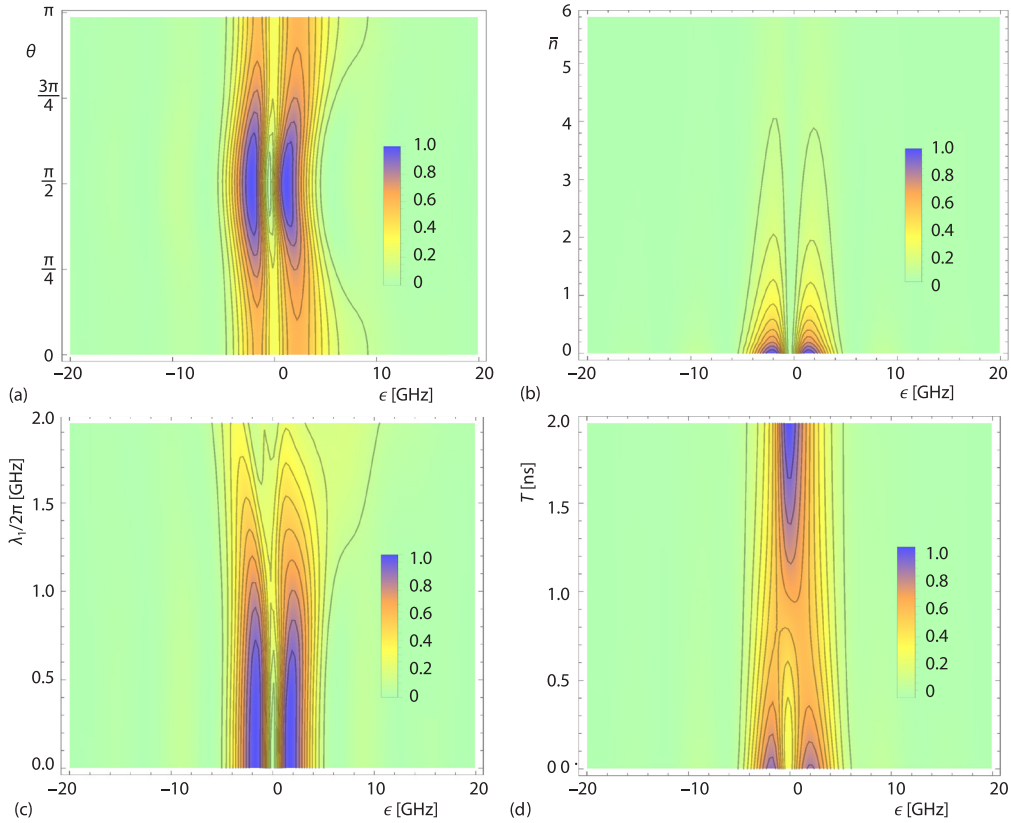


**Figure 3.** The behavior of  $\mathcal{N}_s(\epsilon, T, \gamma)$  for the initial thermal state; (a)  $\lambda_1/2\pi = 0.16$  GHz,  $T = 0.1$ , and  $\bar{n} = 5$ , (b)  $\lambda_1/2\pi = 0.16$  GHz,  $T = 0.1$ , and  $\theta = \pi/4$ , (c)  $T = 0.1$ ,  $\bar{n} = 5$ , and  $\theta = \pi/4$ , and (d)  $\lambda_1/2\pi = 0.16$  GHz,  $\bar{n} = 5$ , and  $\theta = \pi/4$  GHz

## Conclusions

This study investigated the normalized emission spectrum within a hybrid quantum Hamiltonian model integrating atom-photon-magnon interactions. By deriving the effective Hermitian Hamiltonian within the dispersive regime, our focus lay on the atomic normalized emission spectrum originating from the initial excited atomic state, while considering diverse states for the field and magnon-modes, namely, the binomial state, squeezed coherent state, and thermal state.

Our results underscored the substantial reliance of the spectrum on both system parameters and the initial state of the magnon-cavity system. Notably, the spectrum in the  $(\epsilon - \theta)$

plane was predominantly concentrated around zero detuning for small detuning values. In the case of the thermal state, the variation induced by altering the mixing angle remained relatively minor within this region. However, the dependence on the mixing angle became more pronounced when the initial state was either a squeezed coherent state or a binomial state. Specifically, the spectrum exhibited a more pronounced reliance on the mixing angle within the squeezed coherent state compared to the binomial state. Moreover, altering the parameter governing the initial state strength exerted a significant influence.

Across all three studied cases, a gradual decrease was observed with increasing initial state strength, except for the binomial state, where it subsequently increased. Furthermore, the spectrum exhibited a gradual decay without reaching zero in the squeezed coherent state, whereas it decayed and eventually reached zero in the thermal state. Regarding the Magnon-Cavity Coupling, increasing the magnon-cavity coupling resulted in a shift of the spectrum towards higher detuning values. This shift was more pronounced in the squeezed coherent state compared to the other two cases. This behavior was also evident in the time domain, where the spectral shift was more substantial in the squeezed coherent state and absent in the thermal state.

### Appendix A

In this section, we show the detailed derivation for the effective Hamiltonian in eq. (4) using James method [41]. If the physical Hamiltonian in the interaction picture written in the form:

$$\hat{H}_I(t) = \sum_{l=1}^N \left( \hat{K}_l e^{i\omega_l t} + \hat{K}_l^\dagger e^{-i\omega_l t} \right) \quad (A1)$$

where  $\omega_l > 0$  and  $\hat{K}_l$  are the arbitrary harmonic operator with  $l$  number. Then the effective Hamiltonian under the conditions of highly detuned regime in the second perturbation reduces to:

$$\hat{H}_{\text{eff}}(t) = \frac{1}{2} \sum_{r,s=1}^N \frac{\omega_r + \omega_s}{\omega_r \omega_s} \left[ \hat{K}_r^\dagger, \hat{K}_s \right] e^{i(\omega_r - \omega_s)t} \quad (A2)$$

Using the aforementioned equation and interaction Hamiltonian (3), the harmonic operators are:

$$\begin{aligned} \hat{K}_1 &= \lambda_1 \hat{m}^\dagger \hat{a}, \quad \hat{K}_2 = \lambda_2 \cos(\theta) \hat{a} \hat{S}_+, \quad \hat{K}_3 = \lambda_2 \sin(\theta) \hat{a} \hat{S}_z \\ \omega_1 &= \omega_m - \omega_c, \quad \omega_2 = \omega_m - \omega_c, \quad \omega_3 = \omega_c \end{aligned} \quad (A3)$$

By substituting from (A3) into (A2) the effective Hamiltonian can be written:

$$\hat{\mathcal{H}}_{\text{eff}} = \frac{-\lambda_2^2}{\omega_m - \omega_c} \cos^2 \theta (\hat{a}^\dagger \hat{a} \hat{S}_z + \hat{S}_+ \hat{S}_-) + \frac{\lambda_1^2}{\omega_m - \omega_c} (\hat{a}^\dagger \hat{a} - \hat{m}^\dagger \hat{m}) + \frac{\lambda_2^2}{\omega_c} \sin^2(\theta) I + \frac{-\lambda_1 \lambda_2}{\omega_m - \omega_c} \cos(\theta) (\hat{m}^\dagger \hat{S}_- + \hat{m} \hat{S}_+) \quad (A4)$$

### Acknowledgment

This work was funded by the University of Jeddah, Jeddah, Saudi Arabia, under Grant No. (UJ-23-DR-178). Therefore, the authors thank the University of Jeddah for its technical and financial support.

### References

- [1] Mollow, B. R., Power Spectrum of Light Scattered by Two-Level Systems, *Phys. Rev.*, 188 (1969), Dec., pp. 1969-1975
- [2] Sanchez-Mondragon, J. J., et al., Theory of Spontaneous-Emission-Line Shape in an Ideal Cavity, *Phys. Rev. Lett.*, 51 (1983), 1925

- [3] Zhu, Y., et al. Vacuum Rabi Splitting as a Feature of Linear-Dispersion Theory: Analysis and Experimental Observations, *Phys. Rev. Lett.*, 64 (1990), May, pp. 2499-2502
- [4] Agarwal, G. S., et al., Spectrum of Radiation from Two-Level Atoms under Intense Bichromatic Excitation, *JOSA B*, 8 (1991), 5, pp. 1163-1167
- [5] Purcell, E. M., Spontaneous Emission Probabilities at Radio Frequencies, in: *Confined Electrons and Photons*, Springer, Berlin, Germany, 1995, pp. 839-839
- [6] Brune, M., et al., Quantum Rabi Oscillation: A Direct Test of Field Quantization in a Cavity, *Phys. Rev. Lett.*, 76 (1996), Mar., pp. 1800-1803
- [7] Boozer, A. D., et al., Reversible State Transfer between Light and a Single Trapped Atom, *Phys. Rev. Lett.*, 98 (2007), 193601
- [8] Reithmaier, J. P., et al., Strong Coupling in a Single Quantum Dot-Semiconductor Microcavity System, *Nature*, 432 (2004), 7014, pp. 197-200
- [9] Thompson, R. J., et al., Observation of Normal-Mode Splitting for an Atom in an Optical Cavity, *Phys. Rev. Lett.*, 68 (1992), Feb., pp. 1132-1135
- [10] Fu-Li, L., et al., Atomic emission and Cavity Field Spectra of the Jaynes-Cummings Model, *Chin. Phys.*, 12 (2003), 8, 872
- [11] Boca, A., et al., Observation of the Vacuum Rabi Spectrum for One Trapped Atom, *Phys. Rev. Lett.*, 93 (2004), 233603
- [12] Ashraf, M. M., Razmi, M. S. K., Atomic-Dipole Squeezing and Emission Spectra of the Non-Degenerate Two-Photon Jaynes-Cummings Model, *Phys. Rev. A*, 45 (1992), June, pp. 8121-8128
- [13] Feng, J., et al., Emission Spectrum of Two-Mode Non-Linear Jaynes-Cummings Model, *J. Phys. B*, 33 (2000), 22, 5251
- [14] Zhou, Q.-C., et al., Emission and Cavity-Field Spectra in a Cascade Three-Level System Interacting with a Single-Mode Field, *J. Phys. B*, 38 (2005), 23, 4309
- [15] El-Shahat, T. M., et al., Fluorescence and absorption Spectra for A Multi-Photon Jaynes-Cummings in the Presence of Non-Linearities and Stark Shift, *Chaos, Sol. Frac.*, 29 (2006), 2, pp. 262-276
- [16] Obada, A.-S., et al. Treatment of the Emission and Absorption Spectra for a  $\lambda$ -type Three-Level Atom Driven by a Single-Mode Field with Non-Linearities, *Laser Phys.*, 18 (2008), 10, pp. 1164-1175
- [17] Hassan, S. S., et al., Haar Wavelet Spectrum of Sin2-Pulsed Driven Harmonic Oscillator, *Non-Linear Opt. Quantum Opt.*, 48 (2016), 1, pp. 29-39
- [18] Batarfi, H. A., Hassan, S. S., Haar Wavelet Spectrum of an Exponentially Pulsed Driven Qubit, *Non-Linear Opt. Quantum Opt. Concepts Mod. Opt.*, 48 (2017), 2, pp. 93-105
- [19] Li, Y., et al., Hybrid Magnonics: Physics, Circuits, and Applications for Coherent Information Processing, *J. App. Phys.*, 128 (2020), 13, 130902
- [20] Ladd, T. D., et al., Quantum Computers, *Nature*, 464 (2010), 7285, pp. 45-53
- [21] Awschalom, D. D., et al., Quantum Engineering with Hybrid Magnonics Systems and Materials, *IEEE Trans. Quantum Eng.*, 2 (2021), 5500836
- [22] Tabuchi, Y., et al., Coherent Coupling Between a Ferromagnetic Magnon and a Superconducting Qubit, *Science*, 349 (2015), 6246, pp. 405-408
- [23] Lachance-Quirion, D., et al. Hybrid Quantum Systems Based on Magnonics. *Appl. Phys., Express*, 12 (2019), 7, 070101
- [24] Qi, S.-F., Jing, J., Generation of Bell and Greenberger-Horne-Zeilinger States from a Hybrid Qubit-Photon-Magnon-System, *Phys. Rev. A*, 105 ( 2022), 022624
- [25] Alotaibi, M. F., et al., Effects of the Vibrating Graphene Membrane and the Driven Classical Field on an Atomic System Coupled to a Cavity Field, *Res. Phys.*, 31 (2021), 105012
- [26] Alruqi, A. B., et al. Visualization of the Interaction Dynamics between a Two-Level Atom and a Graphene Sheet Covered by a Laser Field, *Alex. Eng. J.*, 77 (2023), Aug., pp. 309-317
- [27] Alruqi, A. B., et al., Entanglement of a Cavity with a Three-Level Atom and a Graphene Membrane in the Presence of a Laser Field, *Alex. Eng. J.*, 75 (2023), July, pp. 419-428
- [28] Li, J., et al., Magnon-Photon-Phonon-Entanglement in Cavity Magnomechanics, *Phys. Rev. Lett.*, 121 (2018), 203601
- [29] Zhang, X., et al., Strongly Coupled Magnons and Cavity Microwave Photons, *Phys. Rev. Lett.*, 113 (2014), 156401
- [30] Zhao, C., et al., Simultaneous Blockade of a Photon, Phonon-, and Magnon-Induced by a Two-Level Atom, *Phys. Rev. A*, 101 (2020), 063838
- [31] Alotaibi, et al., Dynamics of an Atomic System Associated with a Cavity-Optomechanical System, *Res. Phys.*, 37 (2022), 105540

- [32] Zahia, A. A., *et al.*, Bidirectional Field-Steering and Atomic Steering Induced by a Magnon-Mode in a Qubit-Photon System, *Sci. Rep.*, *13* (2023), 1, 14943
- [33] Rao, J., *et al.* Meterscale Strong Coupling Between Magnons and Photons, *Phys. Rev. Lett.*, *131* (2023), 106702
- [34] Lachance-Quirion, *et al.*, Entanglement-Based Single-Shot Detection of a Single Magnon with a Superconducting Qubit, *Science* *367* (2020), 6476, pp. 425-428
- [35] Xiong, W., *et al.*, Optomechanical-Interface-Induced Strong Spin-Magnon-Coupling, *Phys. Rev. A*, *107* (2023), 3, 033516
- [36] Alotaibi, M. F., *et al.*, The Classicality and Quantumness of the Driven Qubit-Photon-Magnon-System, *Mathematics*, *10* (2022), 23, 4458
- [37] Tabuchi, Y., *et al.*, Hybridizing Ferromagnetic Magnons and Microwave Photons in the Quantum Limit, *Phys. Rev. Lett.*, *113* (2014), 083603
- [38] Niemczyk, T., *et al.*, Circuit Quantum Electrodynamics in the Ultrastrong-Coupling Regime, *Nat. Phys.*, *6* (2010), 10, pp. 772-776
- [39] Forn-Diaz, P., *et al.*, Ultrastrong Coupling Regimes of Light-Matter Interaction, *Rev. Mod. Phys.*, *91* (2019), 025005
- [40] Guo, Q., *et al.*, Magnon-Squeezing by Two-Tone Driving of a Qubit in Cavity-Magnon-Qubit Systems, *Phys. Rev. A*, *108* (2023), 063703
- [41] James, D., Jerke, J., Effective Hamiltonian Theory and Its Applications in Quantum Information, *Can. J. Phys.*, *85* (2007), 6, pp. 625-632
- [42] Eberly, J. H., Wodkiewicz, K., The Time-Dependent Physical Spectrum of Light, *JOSA*, *67* (1977), 9, pp. 1252-1261
- [43] Abdel-Aty, M., *et al.*, Fluorescence Spectrum of an Atom Interacting with a Quantized Cavity Field with Arbitrary Non-Linearities, *Int. J. NanoSci.*, *2* (2003), 01-02, pp. 49-63